Chapter-6

Low temperature synthesis of Zinc Ferrite nanoparticles using oxalate based precursor method and its significant effect on the structural and magnetic properties

6.1 Introduction

Nanoferrites are extensively studied by several researchers due to their interesting structural, magnetic and chemical properties compared to bulk ferrites. Nanoferrites have been successfully obtained by numerous preparation techniques such as combustion method [1], citrate method [2], co-precipitation technique using urea [3], titrate precursor method [4], rapid quenched [5], high energy ball milling [6], ceramic method [7], thermal plasma synthesis [8], mechanochemical synthesis [9] etc.

Ferrites are ferrimagnetic materials containing iron oxide as the main constituent with different metal oxides. Ferrites have received considerable attention in experimental, theoretical and computational solid state physics due to their rich and often unusual experimental behavior. Ferrites and substituted ferrites find extensive applications in high frequency devices, RF transformers, toys, TV yokes, and loud speakers and in many of the materials which are used in daily life. Ferrites have greater applications in the current science and technology like in the field of biotechnology for drug delivery, self-assembly and memory devices [10].

The structural and magnetic properties of ferrites depend mainly on the particle size, synthesis techniques and cation distribution. Zinc ferrite is a normal spinel with the tetrahedral (A) sites almost exclusively occupied by Zn^{2+} ions, while the octahedral [B] sites by Fe^{3+} ions and results in normal spinel. Synthesis of nanocrystalline ferrite material like $ZnFe_2O_4$ is growing interest because of wide possible magnetic and catalytic properties. $ZnFe_2O_4$ can be used as starting materials for obtaining substituted ferrites. $ZnFe_2O_4$ is commercially very important magnetic materials having applications such as gas sensors [11], absorbent materials [12] catalyst [13], etc.

Nanocrystalline $ZnFe_2O_4$ has been prepared by several techniques and many interesting results are reported in the literature. In this work nanosized $ZnFe_2O_4$ was synthesized by oxalate based precursor method at very low temperature [14]. It is observed that $ZnFe_2O_4$ shows interesting magnetic properties due to different annealing temperatures. It is observed that $ZnFe_2O_4$ shows ferromagnetic properties below room temperature and paramagnetic above at higher temperatures. Therefore to achieve the ferromagnetic properties of $ZnFe_2O_4$ at and above room temperature we have made an attempt to synthesize the $ZnFe_2O_4$ nanoparticles using oxalic acid based precursor method. In this chapter we will give the explanations about the change in structural and magnetic properties of $ZnFe_2O_4$ nanoparticles with increasing annealing temperature.

6.2 Experimental Procedure

Nanocrystalline powders of $ZnFe_2O_4$ were prepared by oxalate based precursor method. The A.R Grade citric acid ($C_6H_8O_7.H_2O$), zinc nitrate ($Zn(NO_3)_2.6H_2O$), ferric nitrate ($Fe(NO_3)_3.9H_2O$) from sigma Aldrich (≥99%) were used as starting materials. The obtained $ZnFe_2O_4$ nanopowders were annealed at different temperatures 300, 400, 500 and 600 ^{0}C.

The structural characterization of the ferrite powders was carried out using Philips X-ray diffraction system with Ni filter using Cu –Kα radiation (wave length λ = 1.54 A^o). The structural changes with annealing temperature are observed by ABB Bomem MB 102 infrared spectrometer equipped with CsI optics and DTGS detector. The samples were mixed with KBr and made in the form of pellets for IR transmission measurements. The scanning electron micrographs of all samples were taken on JEOL JSM 6360 SEM machine. Room temperature magnetic properties were investigated using Lakeshore VSM 7410.

6.3 Results and discussions

6.3.1. Structural Characterization

Figure 6.1 show the XRD patterns of $ZnFe_2O_4$ nanopowder samples annealed at three different temperatures 300, 400, 500 and 600^0C. The XRD pattern clearly indicates the formation of single phase spinel structure without any secondary phases. It is observed that, as the annealing temperature is increased from 300 to 600^0C, the XRD peaks become sharper and the full width half maximum decreased. The decrease in the full width half maximum is the evidence of increasing the particle size as shown in Figure 6.2. The lattice parameter obtained in our samples are slightly smaller than the standard value reported in JCPDS (card no 79-1150) 8.44 Å. A close look at Figure 6.1 reveals that the intensity of the diffraction lines are increasing and the peaks are shifting towards the higher angles. There are reports available showing that as the inversion parameter increases, lattice parameter decreases [15, 16]. For this reason we have calculated the intensity ratios of 220/400 lines, to find any inversion of cations taking place in our samples with increasing annealing temperature. The intensities ratio of 220/400 lines of our samples showed increasing behavior, this means that there is no inversion of cations with increase in annealing temperature and the cation distribution of prepared $ZnFe_2O_4$ samples corresponds to normal spinel ferrite. This type of behavior was seen in nanosize $ZnFe_2O_4$ with increasing milling time [17].

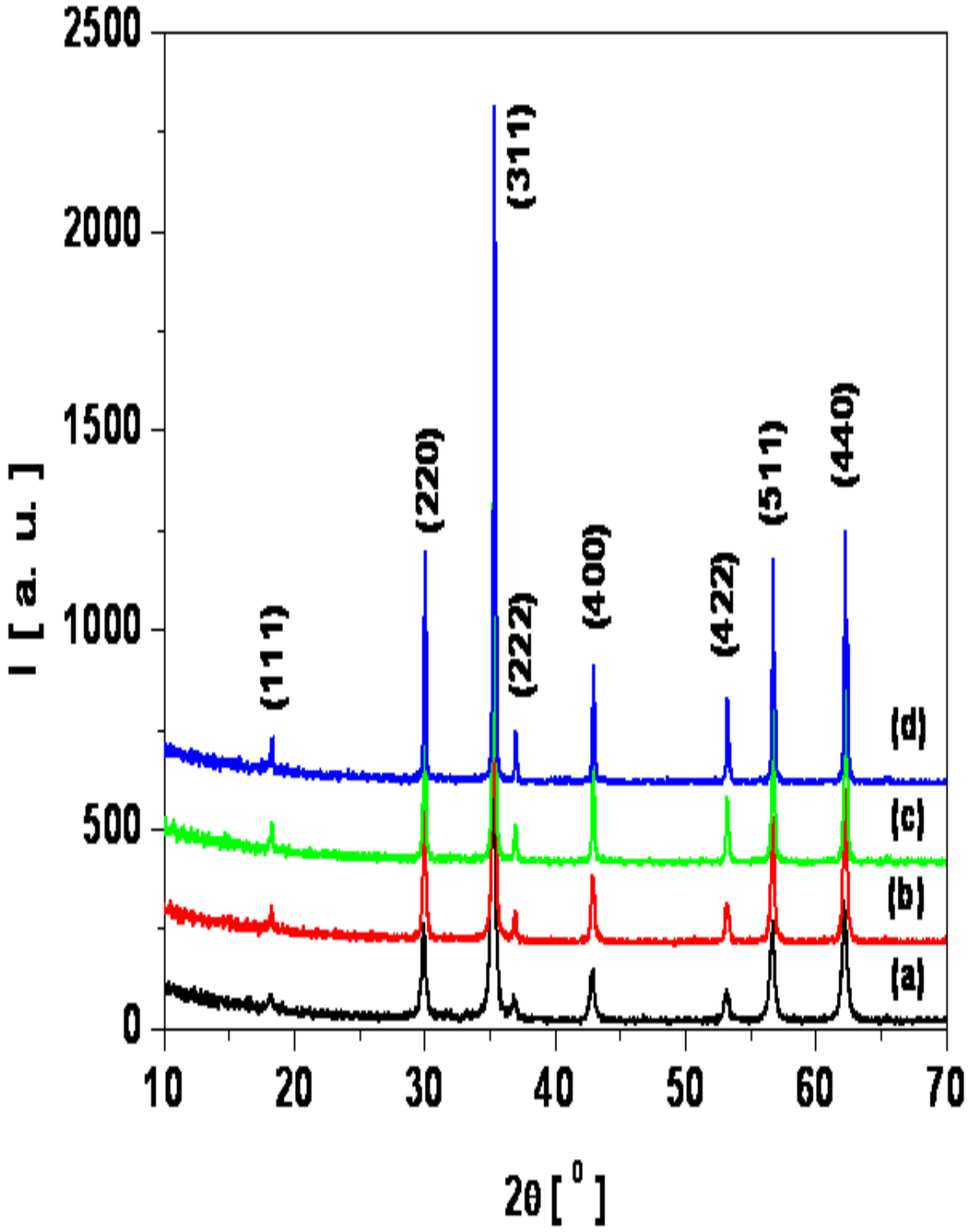

Figure 6.1: X-ray diffraction patterns of $ZnFe_2O_4$ nanoparticles annealed at (a) 300^0C, (b) 400^0C, (c) 500^0C and (d) 600^0C temperatures.

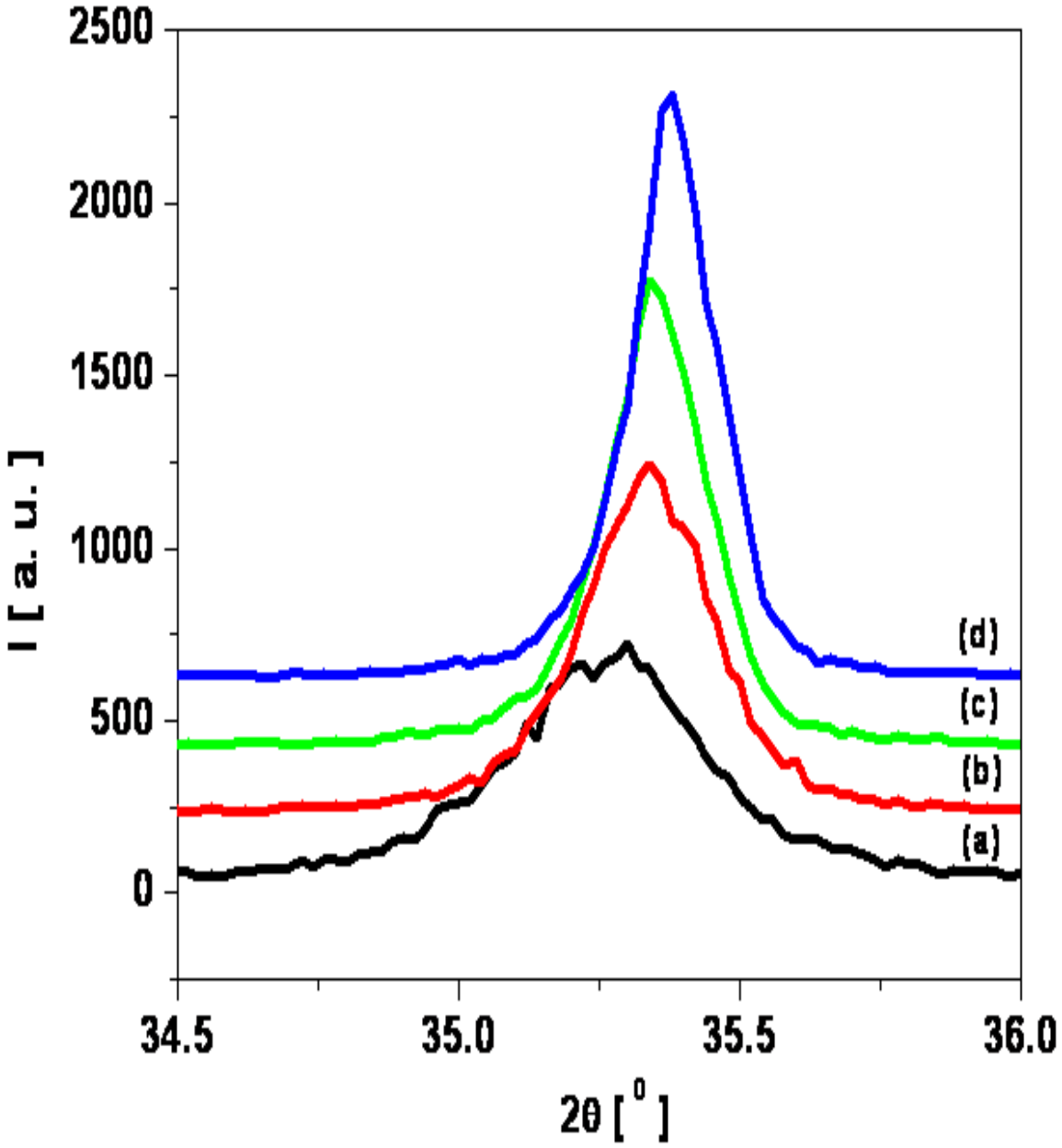

Figure 6.2: X-ray diffraction patterns of most intense (311) peak of $ZnFe_2O_4$ nanoparticles annealed at (a) 300^0C, (b) 400^0C, (c) 500^0C and (d) 600^0C temperatures.

The intensity of XRD peaks increases with annealing temperature showing better crystallinity of the phase. The increase in the intensity of XRD peaks with annealing temperature is due to the formation of crystalline ferrite or may be due to increase in the long-range ordering. This kind of behavior was observed for zinc ferrite samples synthesized by citrate process with aneealing temperatures up to 650^0C. As reported by several authors [2, 4, 7, 8], the formation of well defined crystalline phase of $ZnFe_2O_4$ nanoparticles starts above 450 ^{0}C and is based on the type of synthesis techniques [2]. From our synthesis technique we achieved the single phase $ZnFe_2O_4$ at 300 ^{0}C. Therefore, in the present work the preparation of ferrites around 300 ^{0}C temperature is confirmed by XRD data (Figure 6.1).

It is observed from the XRD data (Figure 6.1) that, as the annealing temperature increases from 300 to 600 ^{0}C, the particle size increases. From Figure 6.2 it is clearly seen that the FWHM is decreasing with increasing annealing temperature as a result the Particle size increases as shown in Table 6.1. It is also observed from Figure 6.2 that, the peak positions shifts with the increase in annealing temperature. The change in the peak position with annealing temperature is attributed due to the change in the lattice constant. In the present case the lpattice constants are observed to decrease with increasing annealing temperature. Also, the decrease in the lattice parameters is also due to the larger ionic radii of Zn^{2+} (0.82 Å) than of Fe^{3+} (0.67 Å). It is observed in ultrafine particles that surface energy and surface tension of particles is high, which results in a tendency to shrink the lattice, which causes reduced lattice constant [18]. Literature suggests that lattice parameters and particle size are directly related; stating that, as particle size increases this causes a corresponding increase or decrease in lattice parameters. From our investigations we found that as the particle size increases with increasing annealing temperature the lattice parameters continue to decrease.

Figure 6.4 (a) and (b) shows the typical SEM micrographs of the Zn ferrite nanoparticles annealed at 300 and 600^{0}C. As seen from the SEM micrographs there is slight agglomeration among particles and the particles are unevenly distributed. Generally in the case of nanoparticles agglomeration is quite expected due to narrow particle size distribution. It is clearly observed

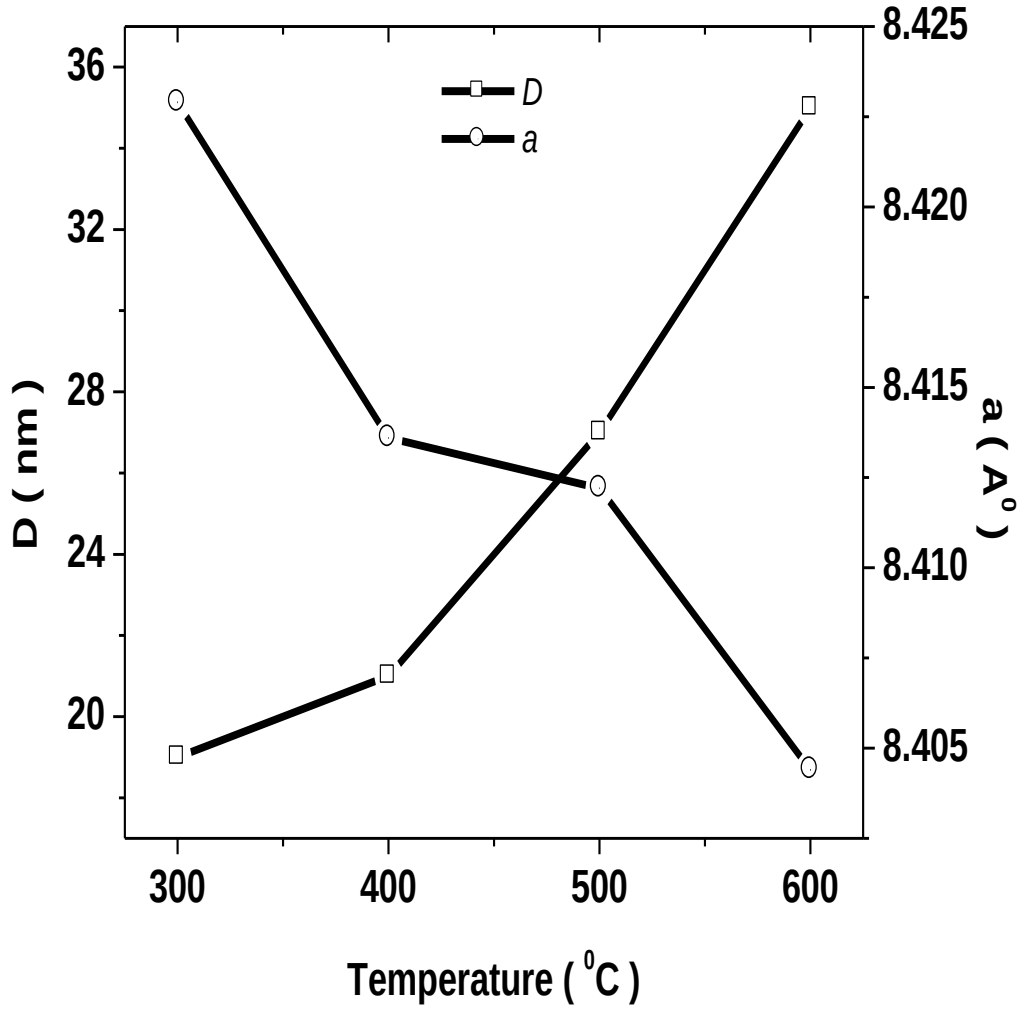

Figure 6.3: Dependence of particle size *D* and lattice constant *a* of $ZnFe_2O_4$ nanoparticles on the annealing temperatures.

from Figure 6.4 (a) and (b) that, there is a significant change in the particle size distribution. As the annealing temperature increased from 300^0C to 600^0C the particle size is observed to increase as observed from the SEM images. Therefore the annealing temperatures promotes for the grain growth. The change in the particle size with annealing temperature as observed from the XRD data is very well in agreement with the SEM analysis.

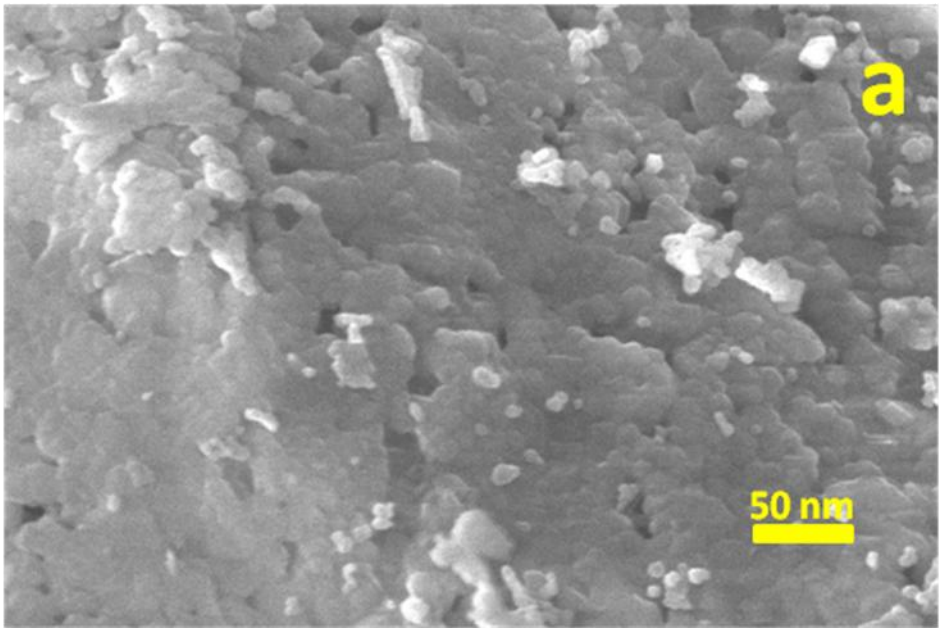

Figure 6. 4(a): SEM micrographs of $ZnFe_2O_4$ nanoparticles annealed at 300^0C

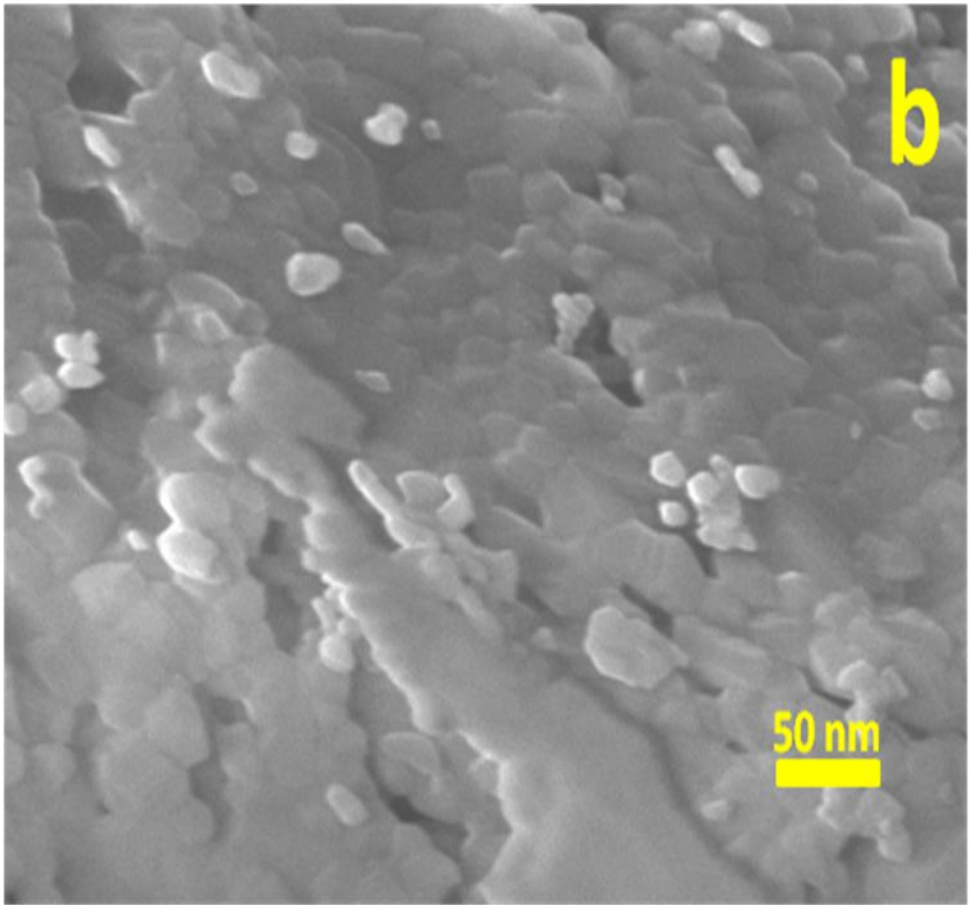

Figure 6.4.(b): SEM micrographs of $ZnFe_2O_4$ nanoparticles annealed at 500^0C.

Table 6.1. Dependent of particle size *D* and lattice constant *a* on the annealing temperature on $ZnFe_2O_4$ nanoparticles

Annealing Temperature (^{0}C)	D (nm)	a (A^0)
300	19	8.4229
400	21	8.4136
500	27	8.4122
600	35	8.4044

The IR spectra of $ZnFe_2O_4$ nanoparticles annealed at different temperatures are as shown in Figure 6.5. It is clearly observed from Figure 6.5 that the IR spectra shows well resolved three absorption bands. The first band, v_1, is located in the 800 – 500 cm^{-1} range, the second band, v_2, in the 500 – 350 cm^{-1} range, while the third band, v_3, occurs between 350 and 280 cm^{-1}. Both v_1 and v_2 are highly asymmetric, actually consisting of several bands. According to interpretation of IR spectra of spinels, given by Waldron [19], v_1 band corresponds to the stretching vibrations of Zn^{2+}-O band in tetrahedral sites, while v_2 is assigned to Fe^{3+}-O stretching of octahedral sites. On the other hand, v_3 is result of oscillations of metal atoms in the isotropic force fields of their tetrahedral or octahedral environment.

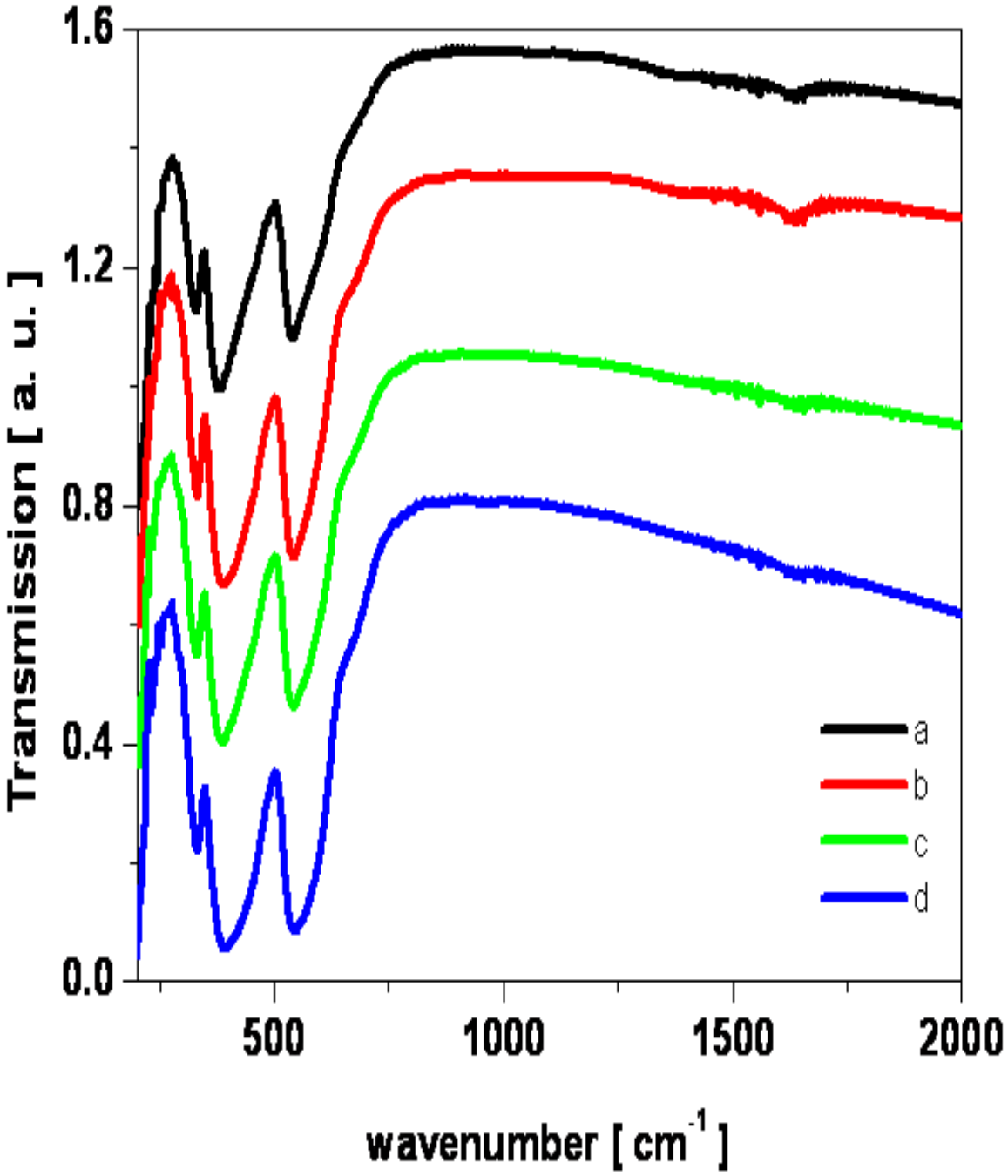

Figure 6.5: IR spectra of $ZnFe_2O_4$ nanoparticles annealed at (a) 300^0C, (b) 400^0C, (c) 500^0C and (d) 600^0C temperatures.

It is evident from Table 6.2 and Figure 6.5 that the v_2 band is the most sensitive with respect to annealing temperatures. It significantly changes its position towards the higher wave numbers with annealing temperature. Simultaneously, it gradually changes its shape, due to the growth of broad shoulder on the high-wave number side of the band [20]. So it can be concluded that the change of the size of nanoparticles causes the variation of positions of v_1 and v_2 infrared bands, which is frequently reported in the literature [21, 22]. These results clearly show that both the tetrahedral and the octahedral sites are affected by annealing temperature. In accordance with XRD measurements, it can be concluded that increase of the annealing temperature improves ordering of the sample with formation of single phase $ZnFe_2O_4$.

Table 6.2: IR data of $ZnFe_2O_4$ nanoparticles annealed at (a) 300^0C, (b) 400^0C, (c) 500^0C and (d) 600^0C temperatures.

Annealing temperature (^{0}C)	v_1 (cm^{-1})	v_2 (cm^{-1})	v_3 (cm^{-1})
300	541	379	331
400	524	386	329
500	538	389	332
600	542	391	333

6.3.2. Magnetic Characterization

The effect of annealing temperature on the magnetic properties of $ZnFe_2O_4$ nanoparticles is shown in Figure 6.6. On increasing the annealing temperature magnetization decreases. Similar results have been reported by P. Uniyal et.al. [23]. this decrease in magnetization with the increase in annealing temperature could be explained on the basis of grain growth. From the XRD analysis, we see that the required phase is formed at 300 ^{0}C. Generally once the required phase is formed further increase in the annealing temperature leads to grain growth. Due to this grain growth, grain traps the inter-granular pores. This inter-granular porosity may lead to decrease of magnetic properties. Magnetically ordered nature of $ZnFe_2O_4$ is evident from the magnetization loops for the samples annealed at 300^{0}C and 400^{0}C.

We have observed the linear magnetization loops for the samples annealed at 500^{0}C and 600^{0}C (see Figure 8). It was reported that, $ZnFe_2O_4$ is antiferromagnetic at room temperature so there should be no additive magnetic contribution at room temperature [24]. The antiferromagnetic spin order of $ZnFe_2O_4$ is not homogeneous. The M-H loops measured for $ZnFe_2O_4$ nanoparticles annealed at 300 and 400^{0}C clearly shows the ferromagnetic behavior. The derived parameters are as shown in Table 6.3. Sample annealed at 300^{0}C shows the maximum magnetization of 9.8 emu/g and for 400^{0}C annealed sample shows 8.6 emu/g. Further for 500 and 600^{0}C samples it is very difficult to find the maximum magnetization as the curves shows linear increasing behavior. For these samples the remanence and coercivity is almost zero, which is similar to the results obtained by other researchers [25, 26].

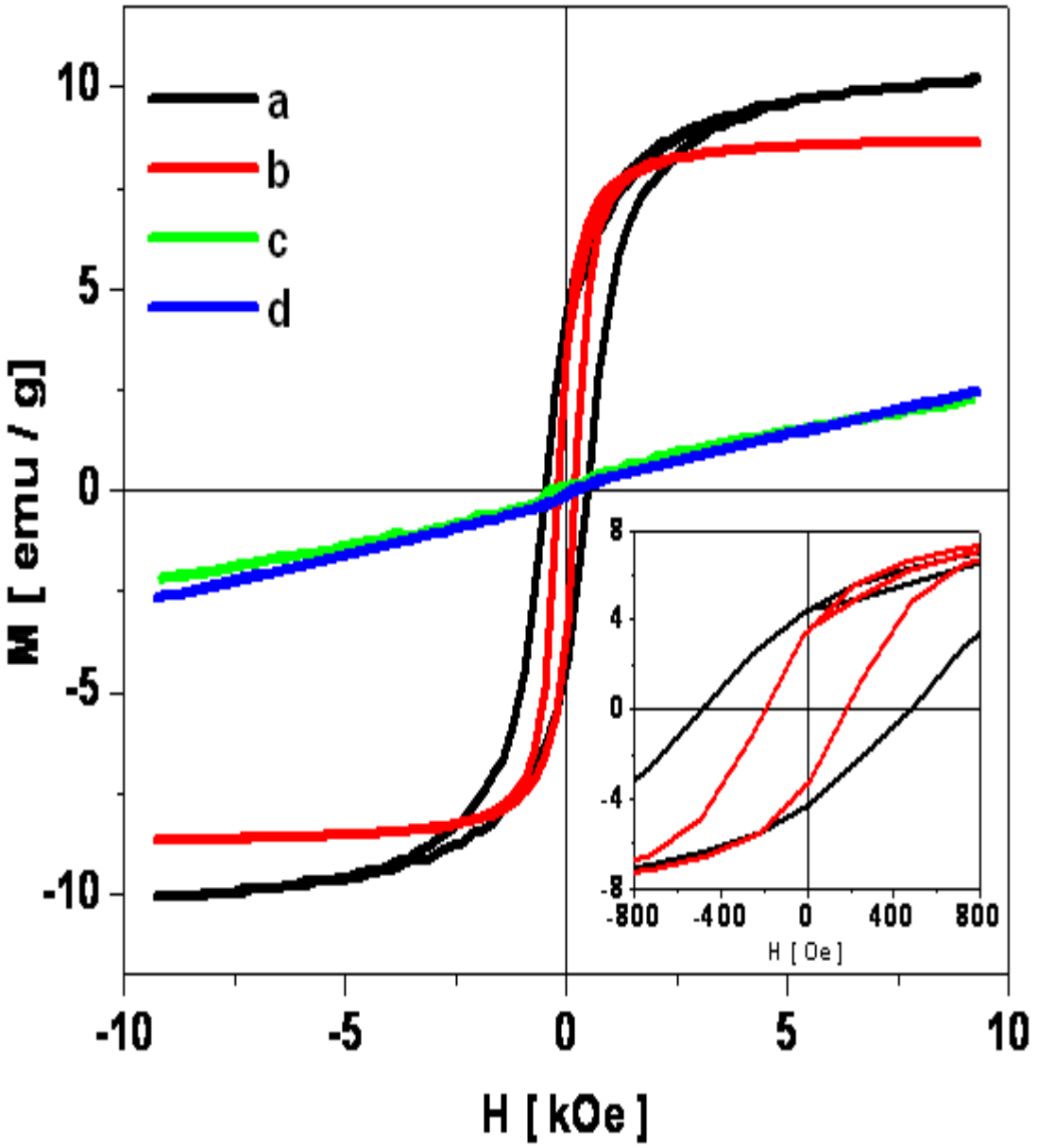

Figure 6.6: Room temperature hysteresis loops at 10kOe for $ZnFe_2O_4$ nanoparticles annealed at (a) 300^0C, (b) 400^0C, (c) 500^0C and (d) 600^0C temperatures.

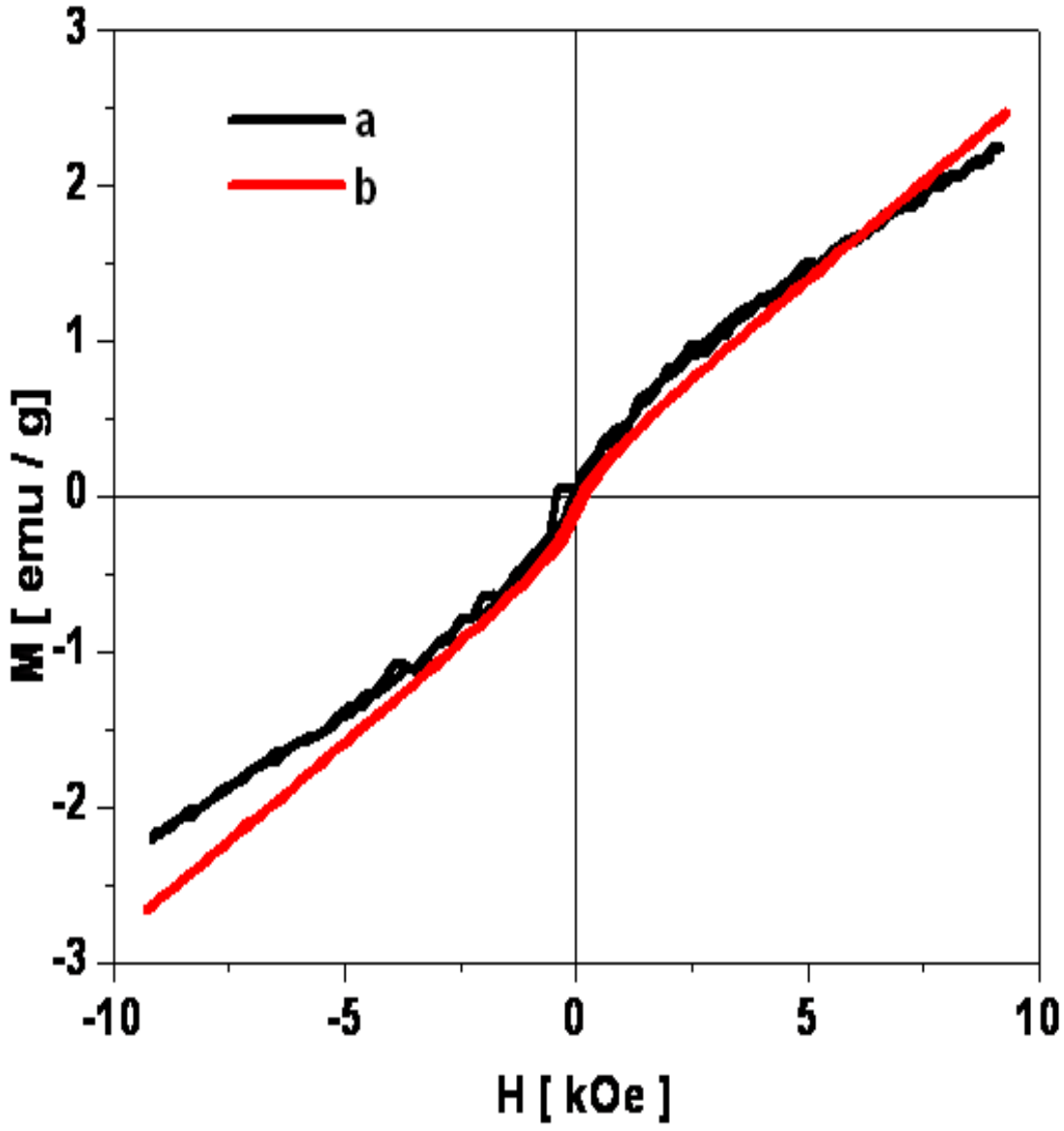

Figure 6.7: Room temperature hysteresis loops at 10kOe for $ZnFe_2O_4$ nanoparticles annealed at (a) 500^0C and (b) 600^0C temperatures.

Table 6.3: Coercivity H_c, remanence magnetization M_r, saturation magnetization for $ZnFe_2O_4$ nanoparticles annealed at different temperatures.

Annealing temperature (^{0}C)	H_c (Oe)	M_r (emu/g)	M_s (emu/g)
300	480	4.42	9.8
400	192	3.41	8.6
500	-	-	-
600	-	-	-

If this surface layer is absent, the magnetization of the particles would saturate with increase in applied field up to a particular magnetic field, when the core magnetic moments align with the magnetic field. At some magnetic field the response of the 'core mode' of the magnetization response is saturated and the core magnetization of the system behaves in a usual Langevin likes way. Beyond this stage any increase in the magnetic field on the particles has an effect only on the surface layer of the particles and thus the increase in the magnetization of the particles slows down [27]. The origin of surface spin disorder for ferrite nanocrystals may be due to broken exchange bonds, high anisotropy layer on the surface or loss of the long-range order in the surface layer.

These effects are particularly strong in the case of ferrites because of the superexchange interaction through the oxygen ions [28]. The magnetization value in our case may be closely related with the existence of magnetically disordered surface layer in which direct completion of exchange interactions between surface spins takes place [29]. Moreover we observed that increase in annealing temperature lead to the decreases in magnetization. Also it is also well known that magnetic properties of ferrites depend on preparation technique.

6.4 Conclusions

Systematic study of structural and magnetic properties of $ZnFe_2O_4$ has revealed that,

1. The nano size zinc ferrite is formed at very low temperature (300 ^{0}C).

2. The particle size was observed to increase with increasing annealing temperature.

3. The IR spectra revealed the existence of the bands; ν_1 band corresponds to stretching vibration of Zn^{2+}-O band in tetrahedral sites, while ν_2 is assigned to Fe^{3+}-O stretching of octahedral sites. On the other hand, ν_3 is result of oscillations of metal atoms in the isotropic force fields of their tetrahedral or octahedral environment. The IR bands shifts towards the lower wavenumbers as the temperature is increased.

6. The magnetic properties of nanocrystalline $ZnFe_2O_4$ compared to multidomain bulk $ZnFe_2O_4$ ferrite can be attributed to the surface effects due to finite size of nanocrystallites.

6.5 References

[1] H. Xue, Z. Li, X. Wang, X. Fu, Mater. Lett. 61(2007) 347.

[2] A.Kundu, S.Anand, H.C.Verma, Powder Technol. 132 (2003) 131.

[3] A. Kundu, C. Upadhyay, H.C. Verma, Phys. Lett. A. 311 (2003) 410.

[4] J.M. Yang, F.S. Yen, J. Alloys Comp. 450 (2008) 387.

[5] K. Tanaka, M. Makita, Y. Shimzugawa, K. Hirao, N. Soga, J. Phys. Chem Solids. 59 (1998) 1611.

[6] S Bid, S.K.Pradhan, Mat. Chem. and Phys. 82 (2003) 27.

[7] L.D. Tung, V. Kolesnichenko, G. Caruntu, D. Caruntu, Y. Remond, V.O. Golub, C.J. O'Connor, L. Spinu, Physica B. 319 (2002) 116.

[8] I. Mohai, J. Szepvolgyi, I. Bertoti, M. Mohai, J. Gubicza, T. Ungar, Solid State Ionics.163 (2001) 141.

[9] V.Nachbaur, G.Tauvel, T. Verdier, M. Jean, J. Juraszek, D. Houvet, J.Alloys.Comp. 473 (2009) 303.

[10] A.G.Roca, R.Costo, A.F.Rebolledo, S.Veintemillas-Verdaguer, P.Tartaj, T.Gonzalez-Carreno, M.P.Morales, C.J.Serna, J.Phys.D : Appl.Phys. 42 (2009) 224002.

[11] X. Niu, W. Du, W. Du, Sensors and Actuators. B. 99 (2004) 405.

[12] F.Toma´s-Alonso, J.M. Palacios Latasa, Fuel Processing Technology. 86 (2004) 191.

[13] J.A. Toledo-Antonio, N. Nava, M. Martınez, X. Bokhimi, Applied Catalysis A: General 234 (2002) 137.

[14] A.T. Raghavender, Shirsath S E, Vijaya Kumar K, J. Alloys. Comp. 509 (2011) 7004.

[15] S. E.Shirsath, B.G.Toksha, K.M.Jadhav, Mat.Chem.Phys. 117(2009) 163.

[16] Q. Chen, A.J. Rondinone, B.C. Chakoumakos, J.Z.Zhang, J. Magn. Magn. Mater. 194 (1999) 1.

[17] S.D. Shenoy, P.A. Joy, M.R. Anantharaman, J. Magn. Magn. Mater. 269 (2004) 217.

[18] T. Sato, IEEE Trans. Magn. Magn. 6 (1970) 795.

[19] R.D. Waldron, Phys. Rev. 99 (1955) 1727.

[20] M. Andrés – Vergés, C. de Julián, J. M. González, C. J. Serna, J. Mater. Sci. 28 (1993) 2962.

[21] T. Suto, K. Haneda, T. Iijima, M. Seki, J. Appl. Phys. A. 50 (1990) 13

[22] F.A. Lo´pez, A. Lo´pez-Delgado, J.L. Mart´ın de Vidales, E. Vila, J. Alloys and Comp. 265 (1998) 291.

[23] P. Uniyal, K.L. Yadav, J.Alloy. Comp. 492 (2010) 406.

[24] A. Verma, T.C. Goel, R.G. Mendiratta, R.G. Gupta, J. Magn. Magn. Mater. 192 (1999) 271.

[25] M. Zheng, X.C. Wu, B.S. Zou, Y.J. Wang, J. Magn.Magn. Mater. 183 (1998) 152.

[26] Q. Chen, J.Z. Zhang, Appl. Phys. Lett. 73 (1998) 3156.

[27] E.Hasmonay, J.Depeyrot, M.H.Sousa, F.A.Tourinho, J.C.Bacri, R.Perzynski, Y.J.Raikher, I.Rosenman, J.Appl. Phys. 88 (2000) 6628.

[28] C.Caizer, M.Stefanscu, J.Phys.D 35 (2002) 3035.

[29] S.Kumar, V.Singh, S.Aggarwal, U.K.Mandal, R.K.Kotnala, Mat.Sci. Engg.B. 166 (2010) 76.